Heating and Trapping of Electrons in ECRIS, from Scratch to Afterglow

A. Heinen*, M. Rüther, H.W. Ortjohann, Ch. Vitt, S. Rhode and H.J. Andrä

Institut für Kernphysik, Universität Münster, Wilhelm Klemm Str. 9, D-48149 Münster, Germany

Abstract

Plasmas in Electron Cyclotron Resonance Ion Sources (ECRIS) are collisionless and the kinetic energy resides in the electrons while the ions stay cold. An ECRIS can therefore be simulated by just following the trajectories of electrons in the confining static magnetic and oscillating microwave electric field. With a powerful algorithm the three-dimensional trajectories of 10^4 ECR-heated and confined electrons are calculated in a standard ECRIS with a deep minimum of $|\boldsymbol{B}|$ and a new ECRIS with a very flat minimum of $|\boldsymbol{B}|$. The spatial electron (plasma) densities and electron energy densities deduced from these trajectories yield new and surprising insight in the performance of ECRIS. The temporal evolution of the electron distributions are shown with and without collision terms, where the latter are responsible for the afterglow effect. The spatial explosion and dilution of the electron density due to relativistic effects will be discussed. New heating methods for optimized electron energy spectra will be suggested.

Although the general behavior of ECRIS could initially be interpreted by considerations borrowed from plasma physics [1], more realistic models can now be developed on the basis of computer simulations. Due to the complex magnetic structure of ECRIS the well known "Particle In Cell (PIC)" plasma physics codes can only be applied in a rotationally symmetric version, so averaging over the very important radial multipolar magnetic confinement. Despite this difficulty impressive results could be obtained with such two-dimensional PIC-code simulation [2]. Most other computer simulations used the fact that the average collision time of electrons in ECRIS is greater than 1 µs, a time which justifies to calculate the free trajectories of electrons in the magnetic confinement of ECRIS. This method was applied quite early to the stochastic resonance heating [3], and has since been used to obtain information on the spatial character of the electron trajectories [4,5]. These calculations were, however, limited to a few trajectories and did not allow for general conclusions. In order to overcome these drawbacks, we are since 1993 developing a code [6,7] which takes into account the full interaction of the electrons with the three dimensional magnetic field and with the microwave (MW) field of single modes in the plasma chamber built as resonance cavity. Wall- and particle-collisions can partially be added. The stochastic MW heating is so fully incorporated and allows to start 10^5 electrons at very low energy of 10 eV of which about 10^4 end up after 1 µs with typical ECRIS electron-energy distributions, electron-spatial density distributions, and -spatial energy density distributions. We have so modeled the ECR plasma and have compared the results to the output ion currents of three ECRIS with different magnetic field configurations and MW resonance modes [6]. Some of the corresponding electron densities and electron energy densities have also been published [7]. Here we present new results on the temporal evolution of the electron distributions without and with collision terms, where the latter are responsible for the afterglow effect. We show the spatial explosion and dilution of the electron density due to relativistic effects with increasing MW power until the resonance zone touches the walls, so creating abundant X-ray production. We include the spatially resolved electron energy spectra and suggest new heating methods for optimized energy spectra and energy densities in ECRIS.

ECRIS plasmas at densities of $n \leq 10^{12}$ cm^{-3} are known to be collisionless [1,6]. The total rate for all electron-electron, electron atom(ion)-collisions is dominated by the ionization of neutrals and is of the order of $\leq 10^6$ s^{-1} at 100 eV and $\leq 10^5$ s^{-1} at 10 keV. A great fraction of the electrons is therefore collisionless for times shorter than 10^{-6} s and can be ECR heated while the ions stay cold at ≤ 2 eV per charge for the ECRIS presented. In such an extreme non thermal equilibrium situation, the free electron dynamics determines to a very good approximation the spatial behavior of the plasma in its magnetic confinement. The ions actually follow the electron density via ambipolar diffusion as a neutralizing background with inertia. All collective plasma phenomena can thus be neglected to first approximation and only the free motion of electrons has to be taken into account in order to obtain the zero order evolution of a plasma inside an ECRIS.

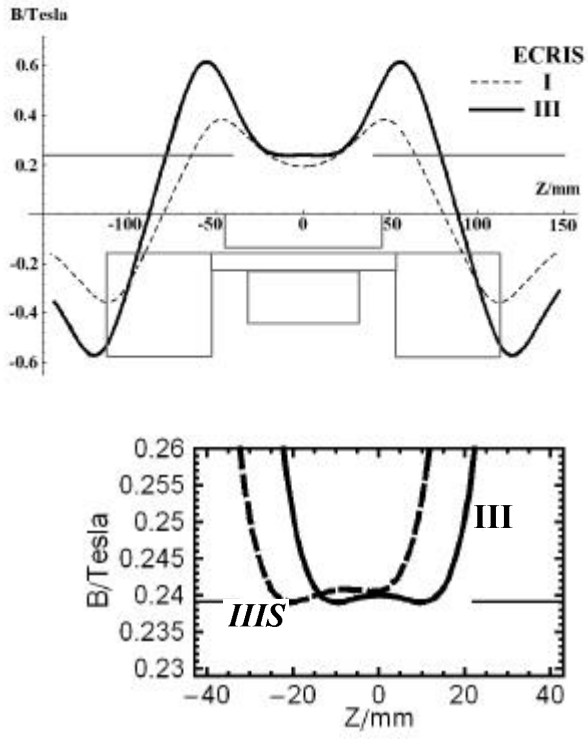

Fig. 1. Magnetic field components B_z on the axis of symmetry of ECRIS I and III with the positions of the radially magnetized rings, the hexapole and the plasma chamber.

* heinen@uni-muenster.de ; http://pikp28.uni-muenster.de/~heinen

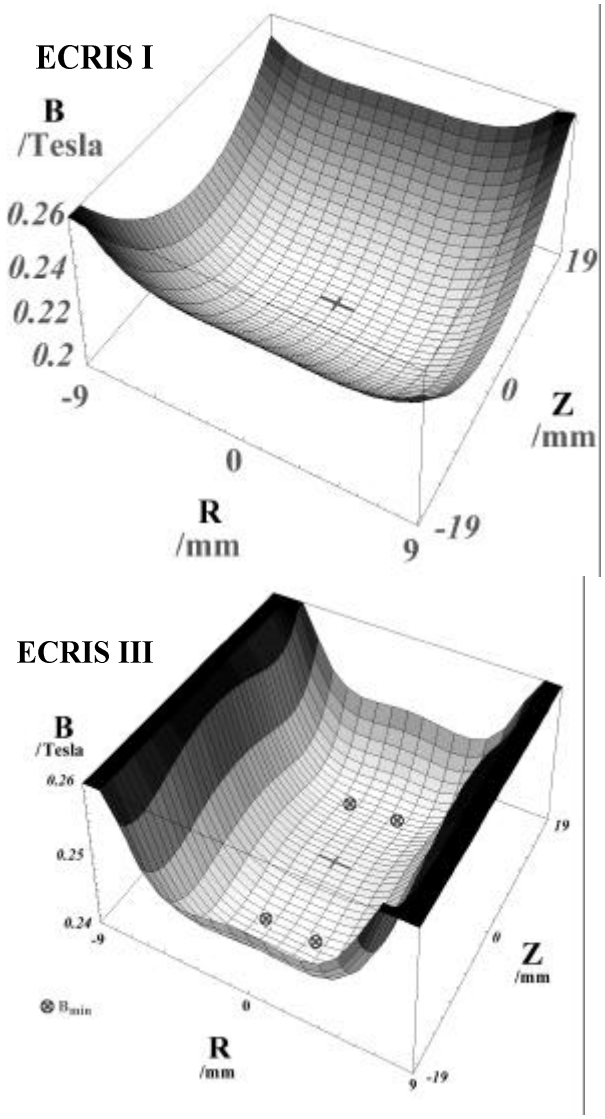

Fig. 2. Magnetic confinement and resonance volume of ECRIS I and ECRIS III.

The low cost, compact, permanent magnet sources ECRIS I and III considered here have been described in [7] of which we recall here the B_z-field in Fig.1 and the magnetic confinement and resonance volume in Fig.2. With a central antenna the E_{012} mode is excited in the plasma chamber which acts as a MW cavity at 6.76 GHz while an off axis antenna excites the H_{113} mode at 6.73 GHz. Fig.3a shows the MW coupling into the plasma cavity on the right via a cooled antenna which is part of a coaxial 7/16 - T shortened on the left. The vertical input is closed by a vacuum window. The horizontal length L of the T is adjusted to 3.75 wave lengths as shown in Fig.3b. The frequency response of the T as measured with the diode shown in Fig.3b is shown in Fig.3c. The response of the T to the variation of L at fixed frequency of 6.7 GHz is shown in Fig.3d while Fig.3e shows the combined response of the T coupled to the plasma cavity according to Fig.3a. The slight splitting of the frequency response in Fig.3e with respect to Fig.3d is well understood as the result of the coupling of two resonators of near equal resonance frequency. With the choice of L a good coupling of the MW into the plasma cavity is achieved. While the empty cavity has a resonance width of 0.15 % the slightly shifted resonance in the presence of the plasma has a width of 1.5 % at a pressure of $2.5 \cdot 10^{-5}$ Pa and a power of 30 W as shown in Fig.3f. The central dip of the measured resonance has to be interpreted as a saturation phenomenon at high central power which is known to reduce the HCI-output of ECRIS, a finding rediscussed later with Fig.12. The latter width is very sensitive to the gas pressure or to the plasma density. It has therefore been systematically measured with the Ar^{1+} - output of a source up to high pressures in Fig.3g. The deduced widths are plotted in Fig.3h and show first a slight increase of the widths with pressure and then a sudden rise at a pressure of $1.3 \cdot 10^{-4}$ Pa. Increasing width implies decreasing MW field amplitude in the cavity so that the plasma density is not increasing linearly with the pressure indicated. On the contrary the plasma density may even drop or stay constant with further increasing pressure. It is probably this the explanation for the leveling off of the width in Fig.3h. We therefore assume that the width would continue to sharply rise at $1.3 \cdot 10^{-4}$ Pa when the plasma density would rise. This behavior has to be interpreted as the cutoff density at 6.7 GHz when taking into account the corrrected pressure inside the cavity which is about a factor of 10 to 20 greater than measured due to the conductances from the cavity to the vacuum gauge. Indeed a factor of 20 would be in agreement with the cutoff density at 6.7 GHz. One therefore has to conclude that even a MW cavity of dimensions of the wavelength of the MW experiences the cutoff density as any other plasma geometry. Since most ECRIS are run at considerably lower pressures, one can conclude also from Figs.3h and 3f that lower pressure implies narrower resonances, i.e. higher Q-values of the cavities and therefore higher MW field strengths. These higher field strengths yield higher electron densities and energy densities in our simulations. These densities are at the origin of a higher production of higher charge states in ECRIS and do so explain why the performances of ECRIS with respect to the output of high charge states generally increase with lower pressures.

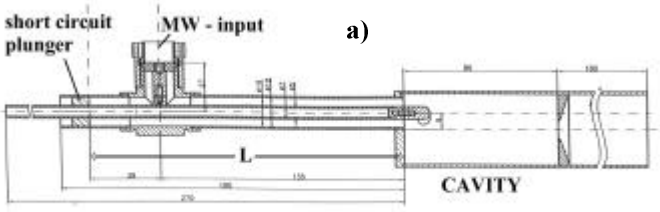

Fig. 3a. 6.7 GHz MW coupling into the plasma cavity.

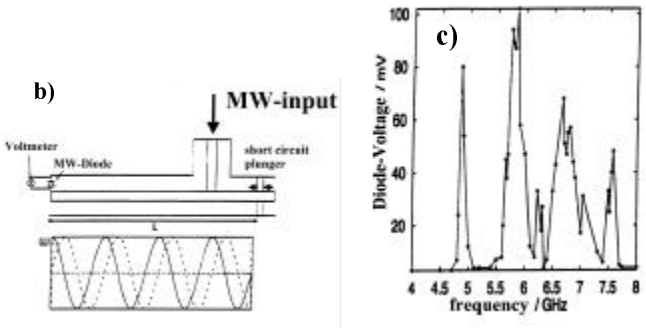

Fig. 3b. Schematic of the MW 7/16 coaxial coupling T-element.
Fig. 3c. Diode voltage versus frequency of the coupling T-element alone with L = 169.4 mm.

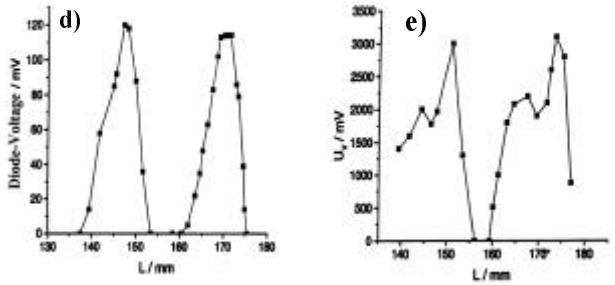

Fig. 3d. Diode voltage versus length L of the coupling T-element at 6.7 GHz.
Fig. 3e. Diode voltage measured at the wall of the cavity (through a small hole) versus length L of the coupling T-element at 6.7 GHz.

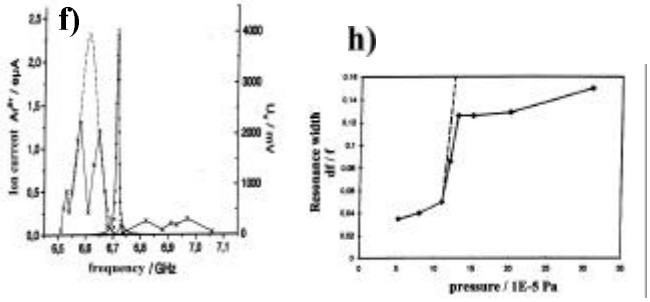

Fig. 3f. Dots: Diode voltage versus frequency measured in the cavity for the completely mounted system of Fig.1 with L = 169.4 mm; Crosses: Ar^{6+} output current versus frequency.
Fig. 3h. The widths of the resonances of Fig.6g versus pressure. The steep rise at $1.2 \cdot 10^{-4}$ Pa is actually much steeper since the plasma density is increasing much less than the pressure due to the fact that the MW amplitude and therefore the plasma heating drops when the width of the resonance increases.

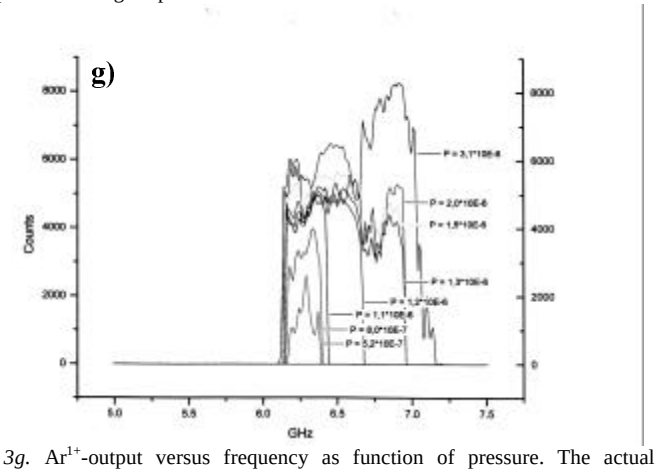

Fig. 3g. Ar^{1+}-output versus frequency as function of pressure. The actual pressure in the plasma cavity is about a factor of 10 greater than shown.

Confined electrons in the ECRIS carry out $6.7 \cdot 10^9$ cyclotron revolutions per second around magnetic field lines at resonance. The relativistic Boris leap-frog algorithm [8] takes advantage of the circular nature of these orbits. It is extended here to include the interaction with the oscillating electric MW field of the resonance mode, so that the ECR heating is completely incorporated. Neglecting collisions, 10 h CPU time of a small workstation are sufficient to pursue 10^4 electrons over a time of 1 μs in order to obtain satisfactory statistics concerning the density, the energy density, and the energy spectra of these electrons. Most results can, however, be obtained within this short simulation time only with artificially increased MW fields. This is justified by the observation that smaller MW fields yield the same results after longer simulation times, as proven occasionally.

As long as electron creation terms in the plasma volume are not incorporated in the program the statistical pursuit of 10^4 electrons can not approach a stationary plasma. The starting conditions of the electrons have therefore to be chosen very carefully as shown in [7]. In general the collisions can completely be neglected for the results presented in this paper. Their important influence on the afterglow will be explained later on. As will be shown for specific examples, the wall interaction does only slightly modify the results for the hot electrons while its influence on the intermediate plasma will be considerable. For the present purposes, it can therefore be assumed that rather realistic hot electron distributions are obtained after 1 μs independent of collisions and wall interactions from which their spatial density and energy density distributions are derived.

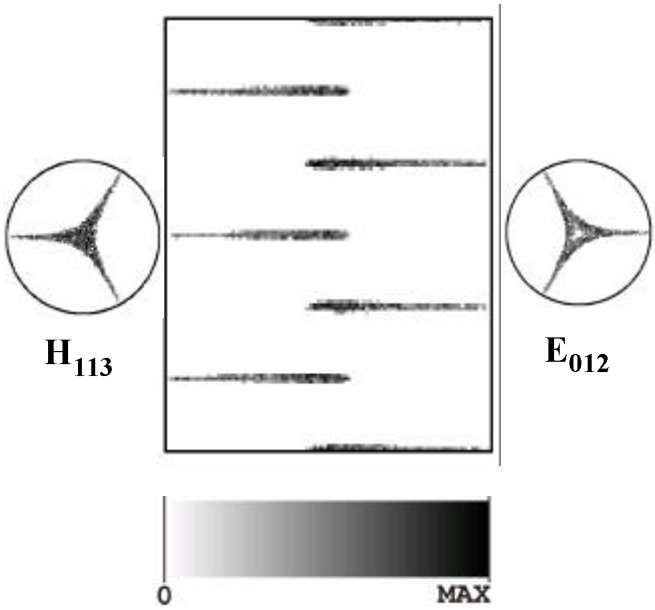

Fig. 4. Impact patterns of electrons on the plasma cavity wall.

By recording all electron impacts on the inner walls of the plasma chamber from T_1 = 900 ns to T_2 = 1 μs after initialization of the trajectories, an impact pattern is obtained in Fig.4 which exactly corresponds to the well known impact or sputtering patterns as observed in all hexapolar ECRIS. It should be noted that these electron impacts stem all from former energetic electrons which were slowed down by the MW in antiphase before they hit the wall. Since only ions can create such traces via sputtering, and ions are supposed to be present and to interact with surfaces where electrons are, this observation is taken as a proof for the appropriate description of the plasma by the present simulation.

In order to obtain the spatial hot electron density inside the ECRIS, the whole volume of the plasma chamber is subdivided into small cubes of 0.5•0.5•0.5 mm^3 and every trajectory is cut into time intervals of 100 ps. After every such time interval within a chosen time window between T_1 and $T_2 > T_1$, the position of the electron is registered and the number of electrons, as accumulated before in the cube at that position, is incremented by one. The repetition and addition of this procedure for all electrons yields a satisfactory statistics for the three-dimensional electron density distribution within the given time windows for the ECRIS under consideration. The energy density can be obtained by using the same procedure, but instead of incrementing the number of electrons in a cube, it is the energy of the electron found in that cube which is added to the energy content, already accumulated before by other electrons in that cube.

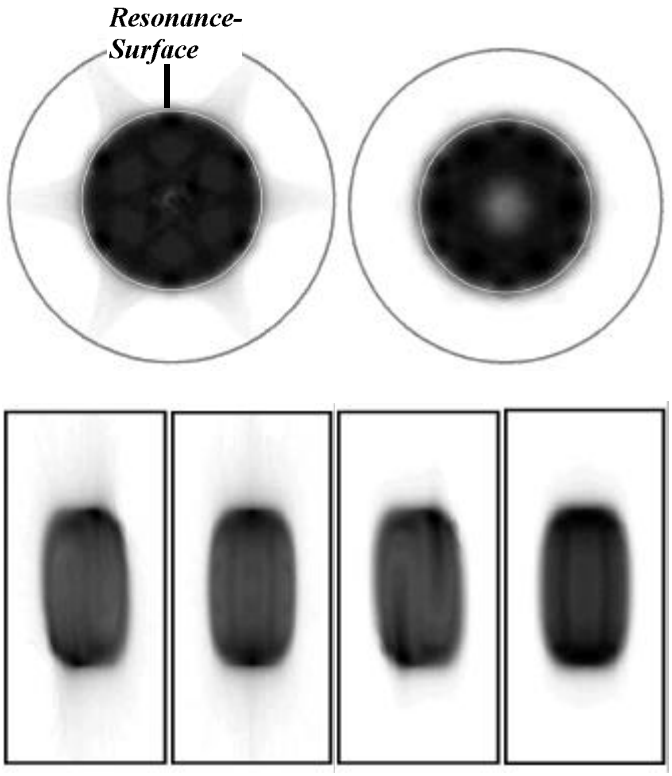

Fig. 5. Projections of the electron distributions of ECRIS I - H_{113} along the symmetry *z*-axis (top) and along the *y*-axis and *x*-axis (bottom). Left: Density. Right: Energy density.

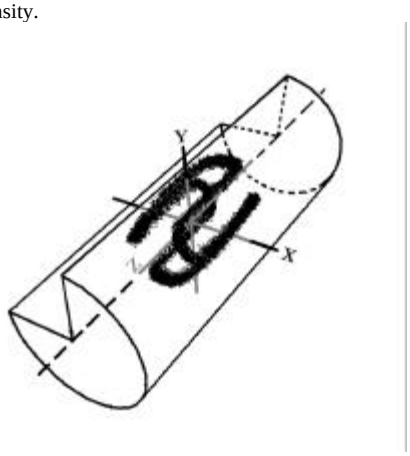

Fig. 6. Typical trajectory wound in loops forming the densities in Fig.5

Fig.5 shows three projections of the spatial density of the electrons with an energy above 20 eV in ECRIS I for the time window 900 ns < T < 1 µs without wall interaction as obtained with a H_{113}-single mode $\boldsymbol{E}(\boldsymbol{r},t) \propto E_0 \cdot \sin \omega t$ with E_0 = 400 V/cm in the plasma cavity after we have shown the corresponding results with the E_{012}-mode in Fig.2 of Ref. [7]. The greatest electron density - a factor of 6 greater than the average density in the cavity - is found within the resonance surface. With respect to the former result with the E_{012}-mode, here the densities are much more homogenous. Only for the energy density a pronounced band of high density wound in loops can clearly be seen. This band is due to typical trajectories of the kind shown in Fig.6 which are quite often obtained when statistically starting electrons close to this band with 10 eV. These electrons are rapidly heated up to >1keV and then stay very stable on the band-like orbits of Fig.6. In these bands the great density of electrons has to be compensated by ions, or in other words the bands form a potential well for attracting and confining great densities of ions. These ions are exposed to the electron energy spectrum in the band as shown in Fig.7 which we assume to be responsible for the production of HCI in these spatial areas.

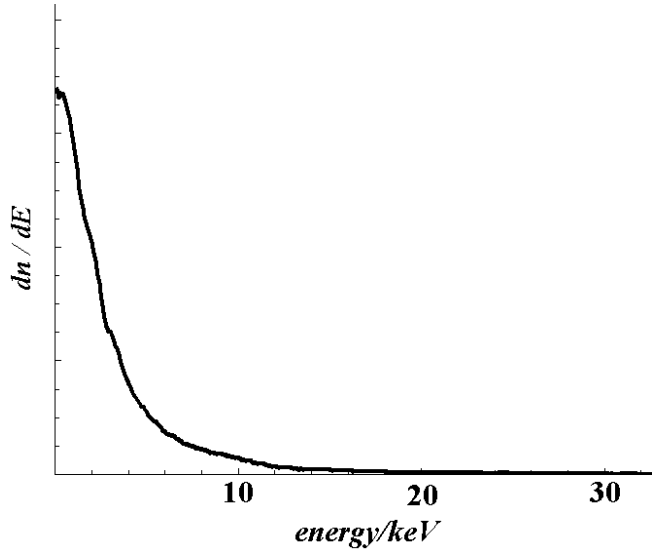

Fig. 7. Electron energy spectrum in the regions of high energy density in ECRIS I - H_{113}

ECRIS III is a new type of ECRIS which is characterized by a great resonance volume instead of a resonance surface, i.e. the volume in which $|\boldsymbol{B}| = |\boldsymbol{B}_{res}|$ (1 ± 0.01) represents a fraction of > 1 % of the volume of the plasma chamber as shown in Fig.2 while a resonance surface constitutes a volume of less than 10^{-4} of the plasma chamber. The electron heating efficiency is thus considerably improved in ECRIS III with respect to ECRIS I. When adjusting the MW frequency to B in the center of ECRIS III, the electron densities and electron energy densities in Fig.8 are obtained.

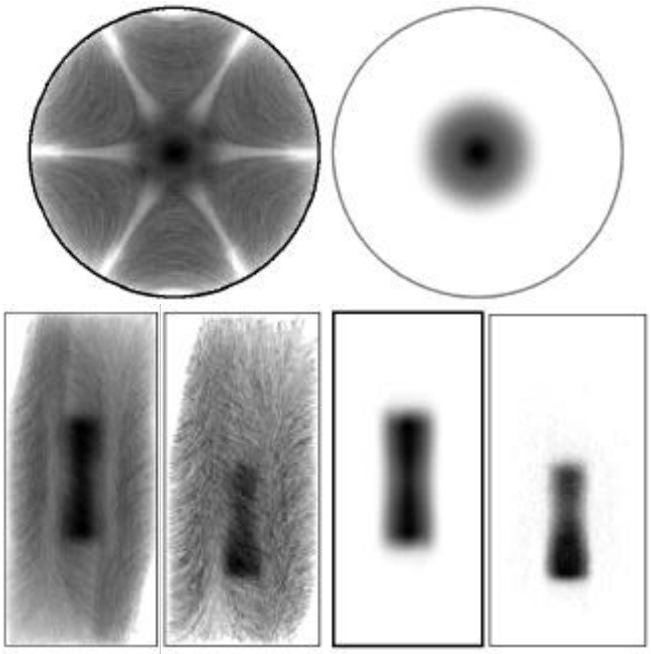

Fig. 8. Projections of the electron distributions of ECRIS III - H_{113} along the symmetry *z*-axis (top) and along the *y*-axis (bottom). Left: Density. Right: Energy density. Every second subfigure at the bottom represents the results of ECRIS IIIS.

The density of the electrons with an energy above 20 eV is concentrated on about 4 % of the volume of the plasma cavity with an even further concentration near the ends of a dumb-bell shaped distribution. The density averaged over the azimuthal angle is shown in Fig.9 with a maximum higher by factor of 30 than the average density in the cavity. The electron energy density is even further concentrated on the dumb-bell within only 3 % of the volume of the cavity. The electron energy spectrum in this volume is shown in Fig.10.

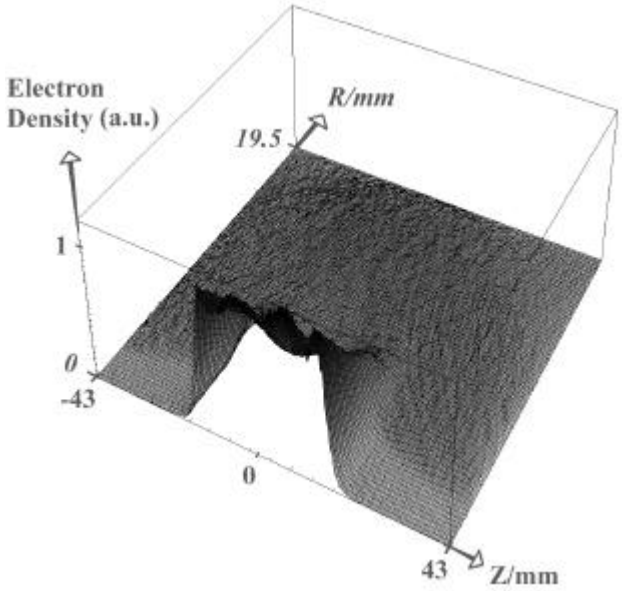

Fig. 9. The azimuthally averaged electron density in ECRIS III - H_{113}

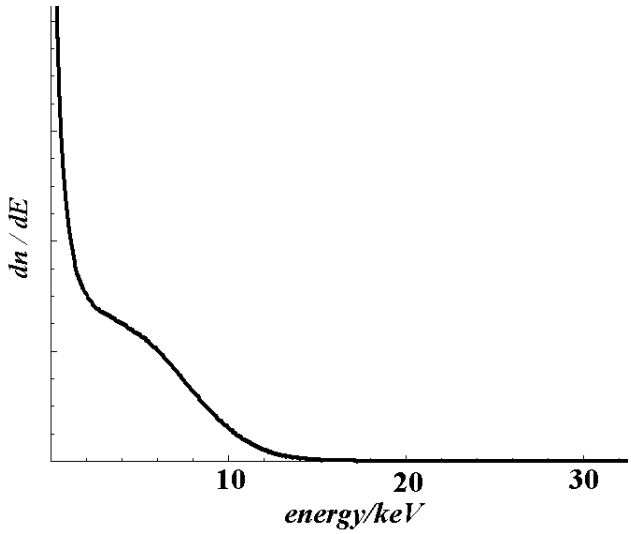

Fig. 10. Electron energy spectrum in the regions of high energy density in ECRIS III - H_{113} at 100 V/cm

Its shape favourably deviates from standard spectra in ECRIS as in Fig.7. Its explanation will appear later on. A very high rate of highly charged ion production can therefore be assumed in this very sharply localized volume. Unfortunately it ends at a distance of about 35 mm from the extraction hole. The HCI, although probably abundantly existing in the dumb-bell, may thus be difficult to extract from ECRIS III. Actually it was necessary to shift the whole electron energy density distribution by 10 mm towards the extraction hole, as also shown in Fig.8 with label IIIS, in order to obtain the very satisfactory results of HCI-currents described in [2]. These HCI currents are extracted with a very small energy dispersion of 1 eV per charge. This is a great advantage for extremely low energy applications, e.g. surface physics, where the full output current can then be decelerated to 1 eV per charge. In order to understand the transport of HCI from their production towards the extraction hole, Ch. Vitt is calculating the spatially resolved HCI charge state distribution inside the cavity on the basis of the above locally resolved electron energy densities and energy spectra. With a transport model for HCI from their point of production towards the extraction hole we hope to complete our modeling of ECRIS with the prediction of performances.

The dumb-bell shaped densities in Fig.8 are essentially results of the relativistic increase of the mass of the electrons with their energy. A non-relativistic calculation would yield sharply concentrated density rings near both ends of the dumb-bell, i.e. in the absolute minima of B of Fig.2. In a relativistic treatment, however, B_{res} will increase with increasing energy of the electrons to $B_{res} = (\omega_{ext}\, m_0 / e)\,(1 + E_{kin} / (m_0 c^2))$ at constant external MW-frequency ω_{ext}. The resonance volume will therefore be transformed into a less efficient resonance surface which climbs up with increasing electron energy the magnetic walls of the confinement and consequently will blow up axially and radially. At moderate MW field amplitudes this effect also stays moderate as shown with Fig.8. When the MW field is further increased, however, the resonance surface will blow up until the confining field limits are reached and the electrons of highest energy hit the walls of the plasma cavity and produce X-rays at energies corresponding to $B_{wall} = B_{res}(E_{kin})$. For instance, the X-rays produced in an ECRIS with $B_{wall} \approx 2 \cdot B_{res} = 0.48$ T would be of the order of 511 keV at 6.7 GHz as actually observed with ECRIS III. It is this relativistic effect which we consider to be responsible for the dilution of the electron density and the rather sudden increase of the X-ray-radiation with MW-power. As a function of the MW field amplitude one therefore expects first an increase of the densities within the resonance surface of ECRIS I up to a maximum from which they drop off with still greater field amplitudes. This behavior can clearly be seen in Fig.11 for the spatial density distributions and in Fig.12 for the density within the resonance surface of ECRIS I as function of MW field amplitude.

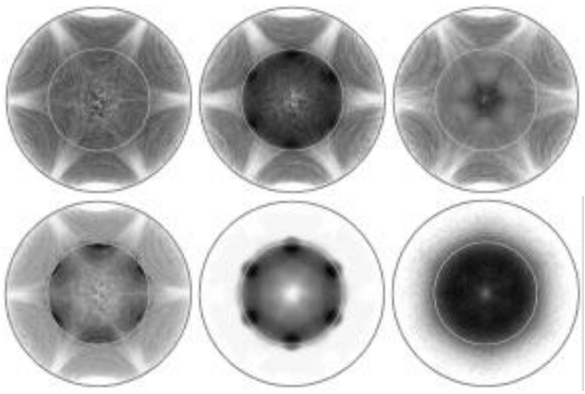

Fig. 11. Dependence of the projection along the z-axis of the spatial electron density (top) and electron energy density (bottom) distribution in ECRIS I on the MW field amplitude of 40 V/cm, 800 V/cm, and 5000 V/cm, respectively from left to right

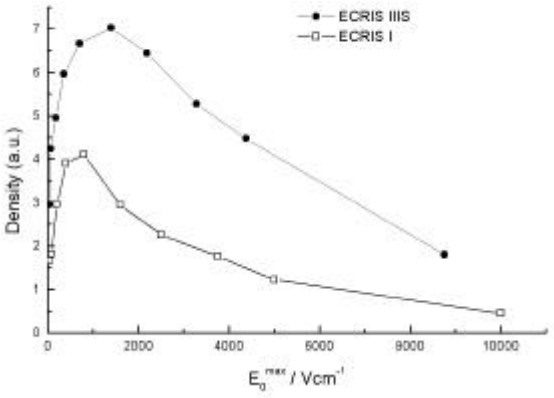

Fig. 12. Electron density within the resonance surface of ECRIS I as function of the MW field amplitude. Note that the field amplitudes are artificially increased ba a factor of about 10 in order to obtain results for 1 µs simulation time.

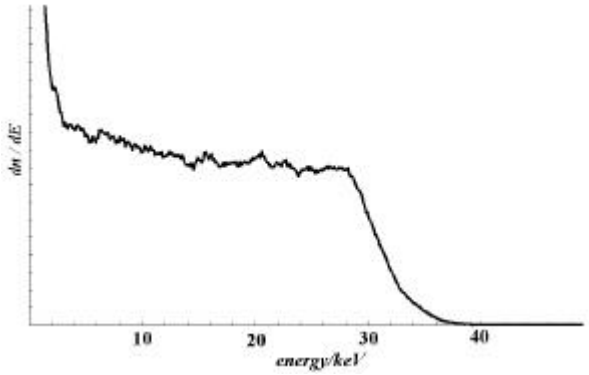

Fig. 13. Electron energy spectrum in ECRIS III run with a hypothetical comb of 20 equally spaced frequencies of 5 % width below 6.6766 GHz in resonance at the center of the resonance volume. Time of simulation is 1 µs.

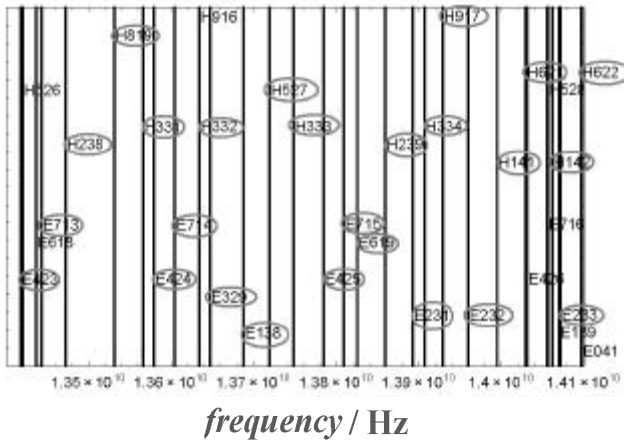

Fig. 14. Spectrum of resonance frequencies of a cavity 80 mm diameter x 190 mm length near 14 GHz

Due to these relativistic effects the great advantage of the great resonance volume of ECRIS III is thus lost with increasing electron energy. In order to restore its advantage one has to keep B_{res} of the magnetic resonance volume constant and has to adjust the MW frequency to the relativistic mass increase $\omega_{ext} = (e\,B_{res} / m_0) / (1 + E_{kin} / (m_0 c^2))$ with E_{kin} of the electrons. For constant B_{res} the external MW frequency ω_{ext} has obviously to be lowered down to some lowest frequency for the highest energy desired in ECRIS. Due to the finite width of the resonances $\delta\omega$ it is then necessary to bridge e.g. the gap $\Delta\omega_{ext}$ between $\omega_{ext}(0)$ for $E_{kin} = 0$ and $\omega_{ext}(25)$ for $E_{kin} = 25$ keV which is 5 % lower than $\omega_{ext}(0)$. For a calculation of the energy spectrum in ECRIS III we have therefore filled a gap of $\Delta\omega_{ext} / \omega_{ext}(0) = 0.05$ by 20 equally spaced frequencies with 100 V/cm each, as if it were possible to couple all these frequencies into the mono-mode cavity of ECRIS III. The energy spectrum of Fig.13 is obtained which offers fantastic advantages over the standard spectra in ECRIS for the production of high charge states. For its realization, it is thus necessary to use multi-mode cavities which allow for sufficiently close resonances in order to cover $\Delta\omega_{ext}$. A plasma cavity of 80 mm diameter and 190 mm length fulfills this requirement near 14 GHz for which the eigen-modes are shown in Fig.14. By choosing 23 of these modes as input frequencies one obtains the density distributions of an ECRS III (14 GHz) adapted to field strengths for 14 GHz in Fig.15. Compared to the calculation for the same source with a single MW frequency at $\omega_{ext}(0)$ in Fig.16, the results in Fig.15 show striking differences and advantages. The excellently flat energy spectrum up to 25 keV with relatively sharp cutoff is very well adapted to the production of high charge states. The density and energy density distributions are much more concentrated on both ends of the dumb-bell as compared to Fig.8 and 16 where they form rings around the axis, however. These high densities together with the energy spectrum promises a very efficient production of very high charge states. We therefore propose this new source design for future high performance ECRIS. It is particularly attractive because it allows to shift the cutoff energy of the energy spectrum to any desired value by choosing ω_{extmin} of the comb of frequencies. The cutoff function of the spectrum can furthermore be controlled by the power per frequency which is responsible for the resonance width of each frequency. Small power yields narrow resonances $\delta\omega$ and sharp cutoff but requires a great number $\Delta\omega / \delta\omega$ of frequencies. Great power yields large $\delta\omega$ and a soft cutoff but requires a smaller number of frequencies. In the limit of very great power $\delta\omega$ can approach $\Delta\omega$ so that a single frequency allows to roughly approximate the spectrum of Fig.15. This most simple technique, however, has its limits due to the dilution and X-ray effects discussed with Figs.11 and 12. Finally it should be mentioned that the frequency comb technique may efficiently be applied (and has been applied with two frequencies) to existing standard ECRIS. Their electron energy spectra and densities can be considerably improved but not to the quality of Fig.15.

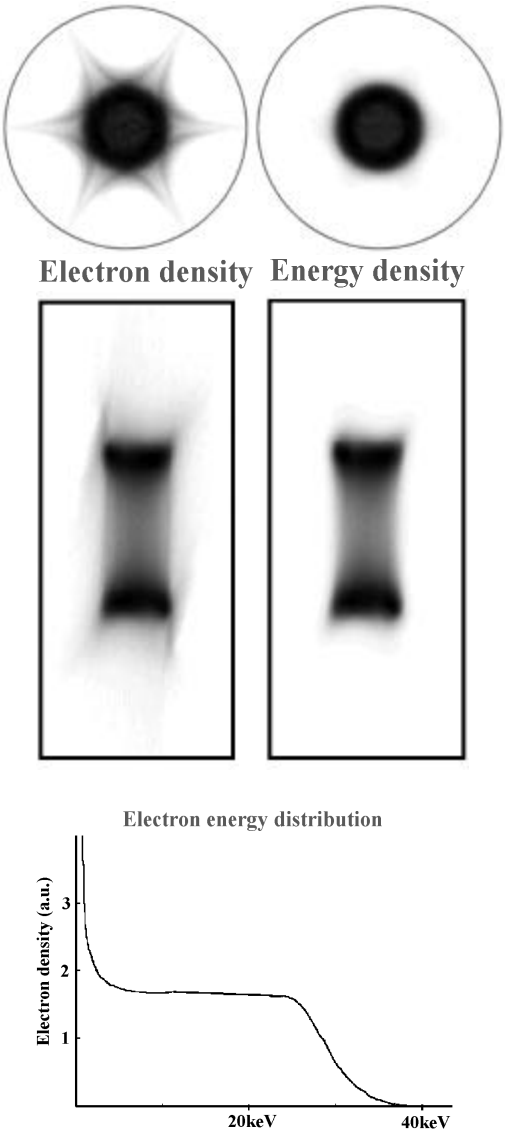

Fig. 15. Projections of the electron distributions of ECRIS III (14 GHz) along the symmetry *z*-axis (top) and along the *y*-axis (bottom). Left: Density. Right: Energy density. The source is run with 23 frequencies as indicated in Fig.14 with a field of 100 V/cm each. Simulation time: 1 μs

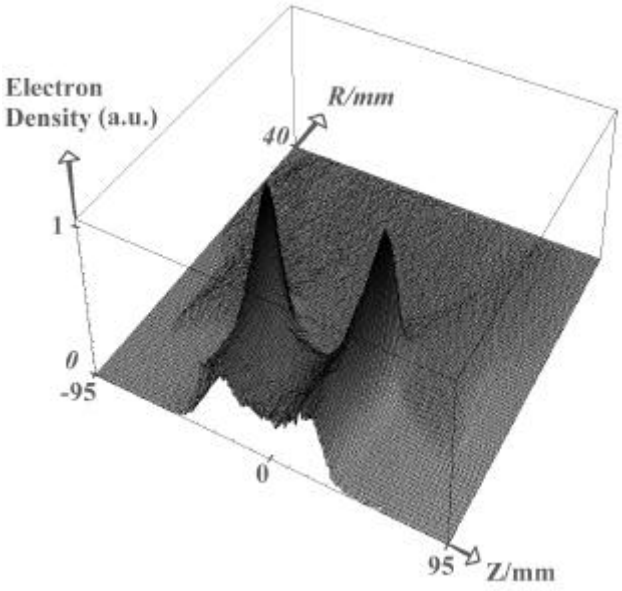

Fig. 15b. The azimuthally averaged electron density in ECRIS III (14 GHz)

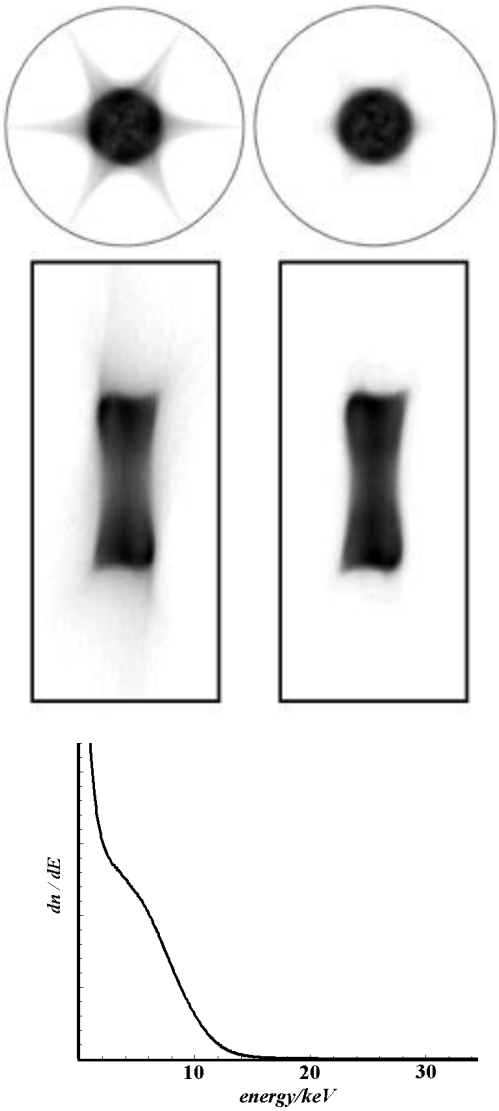

Fig. 16. Same as Fig.15 but run with a single frequency in resonance at the center of the resonance volume.

Collisions have been completely neglected up to now. This is perfectly justified by the short simulation times with respect to the collision times. Collisions are expected to play a role only on time scales of milli seconds or more. In order to approach this scale we have to use a sort of quick motion picture technique by artificially increasing the density of the collision partners by a factor of 1000 to 10^{15} cm^{-3}. With this technique collision phenomena taking place on a ms scale in real ECRIS can be observed in our simulations and are presented on a ms scale in Fig.17. It is impressive to see the same densities build up in ECRIS I as without collision terms as long as the MW interaction restores the electron trajectories after every collision as shown in Fig.17a. With this density distribution installed, the MW is switched off so that we can now observe the afterglow of ECRIS in Figs.17b at 0.25 ms, 17c at 2 ms, and 17d at 4 ms after the MW switch off. Right after the switch off in particular the low energy fraction of the initial density concentrated within the resonance surface suddenly explodes and leaves at first the heavy HCI`s behind. They do in turn also Coulomb-explode towards the walls and in particular towards the extraction hole, a direction which is favored by the magnetic structure, giving rise to the temporary

peak of high intensity of HCI. During this early stage of the afterglow the high energy part of the electron spectrum in Fig.18 is only little affected so that the diffused density distributions in Fig.17c,d can persist over long times on a ms scale. The ECRIS thus continues to work with HCI-output the charge state distribution of which shifts, however, to lower and lower charge states with time due to the continuous decrease of the density and energy density. Fig.18 thus confirms earlier models [1] of the afterglow effect while Figs.17 and 18 do give us now a deeper and more precise insight into the spatial and temporal behavior of the electrons during the afterglow.

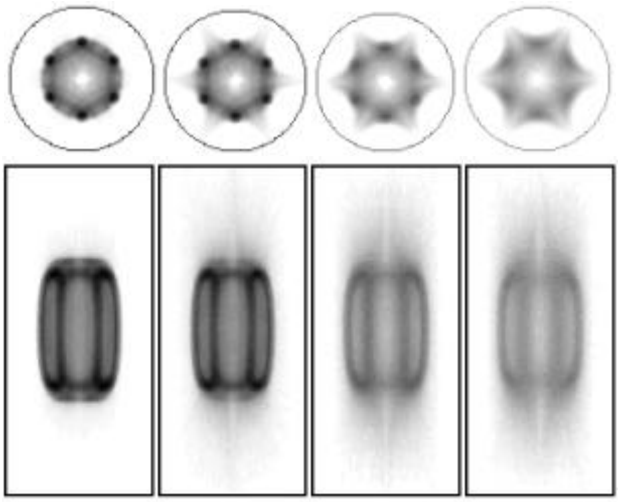

Fig. 17. The afterglow: Projections of the electron density distributions of ECRIS I along the symmetry *z*-axis (top) and along the *y*-axis (bottom). From left to right: Before switch off, 0.25 ms, 2 ms, and 4 ms after switch off of the MW

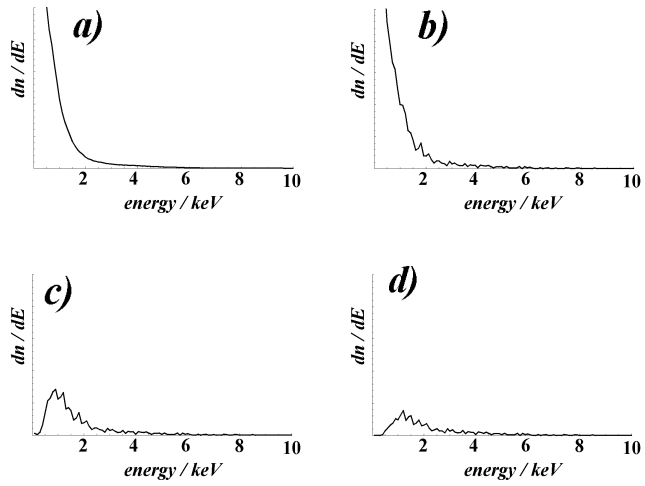

Fig. 18. The afterglow: Electron energy spectrum as function of time**.** a) before switch off , b) 0.25 ms, c) 2 ms, and d) 4 ms after switch off of the MW

To recall, all these results have been obtained by neglecting collective phenomena, of which the most important one is probably the diamagnetism of the electrons. At the densities discussed here the diamagnetism could amount to 5 to 10 % and will modify some of the results in a future calculation including it. Nevertheless, with the present it is shown that our simulations can provide deeper and new insight into the physics of an ECRIS. The good description of many phenomena encourages us to propose a new design of a very efficient and performing great resonance Volume-Frequency-Comb - VFC-ECRIS as outlined for Fig.15. Pushed to B_{res} = 1 T at 28 GHz one could achieve unprecedented electron and electron energy densities for the production of extremely high charge states. Its HCI-output could be further improved by the ECRIS IIIS - technique of Fig.8 and by a fast and periodic magnetic lowering of the confinement near the extraction. Such an VFC-ECRIS should be a challenge for all of us.

This work is **not** supported by the Deutsche Forschungs Gemeinschaft.

References

[1] R.Geller, “Electron Cyclotron Resonance Ion Sources and ECR Plasmas”, IOP Publishing Ltd. (1966) and 491 references therein.

[2] G.D.Alton and D.N.Smithe, Rev.Sci.Instr. **65**, 775 (1994).

[3] Y. Jongen, in 6th Int. Workshop on ECR Ion Sources (Berkeley, CA,USA, 1985), ed. C. Lyneis, LBL, P.U.B. 5143.

[4] S. Biri, Calculations with the TRAPCAD-code; see e.g. J. Vamosi and S. Biri, Comput. Phys. Commun. **98**, 215 (1996).

[5] P. Sortais, private communication.

[6] A. Heinen, M. Rüther, J. Ducrée, J. Leuker, J. Mrogenda, H.W. Ortjohann, Ch. Vitt, E. Reckels, and H.J. Andrä, Rev.Sci.Instr. **69**, 729 (1998).

[7] A. Heinen, Ch. Vitt, and H.J. Andrä, in Conference on the Physics with Highly Charged Ions, Bensheim, Germany Sept. 1998, to be published in Physica Scripta.

[8] “Plasma Physics via Computer Simulation”, eds. C.K.Birdsall and A.B.Langdon, IOP-Publishing Ltd. (1995).